Klyatskina, E.; Rayón Encinas, E.; Darut, G.; Salvador Moya, MD.; Sánchez, E.; Montavon, G. (2015). A study of the influence of TiO2 addition in Al2O3 coatings sprayed by suspension plasma spray. Surface and Coatings Technology. 278(25):25-29. doi:10.1016/j.surfcoat.2015.07.029.

A study of the influence of TiO_2 addition in Al_2O_3 coatings sprayed by Suspension Plasma Spray

E. Klyatskina[1], E. Rayón[1], G. Darut[2], M. D. Salvador[1], E. Sánchez[3], G. Montavon[2]

[1] Instituto de Tecnología de Materiales, Universitat Politécnica de Valencia, Cami de Vera, s/n, 46022 Valencia, Spain

[2]LERMPS-EA3316, Université de Technologie de Belfort-Montbéliard, site de Sévenas, 90010 Belfort Cedex, France

[3] Instituto de Tecnología Cerámica, Campus Universitario Riu Sec, Avda. de Vicent Sos Baynat s/n 12006 Castellón Spain

Corresponding Author:

Name: Elizaveta Klyatskina

Phone: +34 660806113

E-mail: elkl1@upvnet.upv.es

Postal Address:

Instituto de Tecnología de Materiales.

Universidad Politécnica de Valencia.

Camino de Vera s/n. E-46022. Valencia

Spain

Abstract

In this work, five different concentrations of a mixture of TiO_2/Al_2O_3 nanopowders in an alcoholic suspension at 10%wt solid content were sprayed by Suspension Plasma Spraying on steel discs. The influence of the presence of TiO_2 at 0, 13, 40 and 75 %wt in Al_2O_3 was analyzed by studying the properties of the sprayed coatings. Microscopy analysis of the projected coatings revealed a homogeneously distributed microstructure, where the densification of the coating increases with TiO_2 content, while the original nanostructure is maintained. A nanoindentation study revealed an increment of nanohardness and elastic modulus due to the densifying effect of TiO_2. The addition of significant amounts of TiO_2 has been revealed as necessary in order to favour the fusion of Al_2O_3 in the SPS process.

Keywords: Coating densification, alcoholic suspension, Suspension Plasma Spraying, Al_2O_3 - TiO_2, Nanoindentation.

1. Introduction

Nanostructured ceramic coatings possess better mechanical properties, such as toughness and hardness, than conventional ceramics, as well as chemical resistance and yield stress due to a diminished grain size [1-6]. Nowadays, a bulk ceramic piece with a nanostructured microstructure can be produced by sintering nano-sized powders via fast routes (to prevent grain growth) such as microwave furnaces [7,8] or Spark Plasma Sintering techniques [9,10]. However, in order to produce ceramic coatings onto a substrate by utilizing

powders as feedstock, the most employed technique is Atmospheric Plasma Spraying (APS) [11,12]. This technique consists in injecting powder into a plasma plume. The feedstock is then molten by the high temperature of the plasma as it is accelerated towards a substrate, where the material solidifies augmenting the coating thickness. Nevertheless, when a nanometric-sized powder is sprayed, the small masses and large specific surface area of the particles lead to a loss of acceleration in the plume flux and, consequently, the projected material fails to reach the substrate or does so with insufficient energy [13,14].

The provided solution to obtain coatings using nanopowders in plasma spraying is to inject the nanoparticles inside the plasma plume by means of a liquid carrier instead of a gas [15,16]. This technique is known as Suspension Plasma Spraying (SPS) because nanoparticles are within a liquid suspension instead of the conventional dry process.

Several reports have demonstrated that nanometric ZrO_2 [17,18], TiO_2 [19-21] and Al_2O_3 [22,23] are successfully deposited by SPS. The SPS coatings obtained using nanopowder feedstock exhibit superior characteristics due to the fact that they present a much lower porosity, leading to a denser structure. The most common SPS applications include thermal barrier coatings, wear and abrasive protection coatings, biocompatible coatings and corrosion protective coatings [24].

In the particular case of alumina, it presents a high melting point and, in powder form, it is able to reach nanometric particle sizes. The literature reports that low density coatings with low cohesion and high porosity [25] can be obtained. Improving the quality of Al_2O_3 coatings is of special interest because of its

exceptional wear resistance properties [26-28]. In this sense, researchers are focusing their attention to find the experimental SPS conditions to obtain denser alumina coatings while maintaining the nanostructure. The best result achieved in alumina coatings obtained by SPS involves the addition of low quantities of titania, e.g. Al_2O_3 with 13 %wt TiO_2 [28]. It was found that titania acts as a flux agent and its presence improves the resultant mechanical features of coatings. Reports based on the study of the evolution of coating properties under different TiO_2/Al_2O_3 contents have been found, but none of them using an alcoholic suspension of 10 %wt solid content.

The aim of this work is to obtain several TiO_2/Al_2O_3 coatings by SPS varying the concentration of TiO_2 with respect to Al_2O_3 in an alcoholic suspension of 10 %wt solid content. The evolution of the microstructure and the nanomechanical properties of the obtained coatings are analyzed by electron microscopy and nanoindentation techniques.

2. Experimental Procedures

2.1 Process and related operating parameters

A F4-MB torch (Sulzer-Metco, Wohlen, Switzerland) equipped with a 6 mm internal diameter anode nozzle was employed for coating growth. The suspension momentum upon penetration into the plasma flow is controlled by adjusting the pressure inside the container where the suspension is stored. The plasma arc was maintained by a constant current intensity of 600 A. The gas was a mixture of Ar 40 slpm and He 20 slpm. The kinematic parameters were: torch scan velocity of 1 $m \cdot s^{-1}$, scanning step of 10 mm $pass^{-1}$ and spray

distance of 30 mm. The mass enthalpy of the plasma remained at a fixed level of 14.5 $MJ \cdot kg^{-1}$during the coating process.

Low-carbon steel discs of 25 mm diameter were used as substrates. Surfaces were previously polished by a sequence of abrasive SiC paper and diamond slurries in order to achieve surfaces with an average roughness, R_a = 0.7 μm. Subsequently, substrates were degreased with acetone and cleaned with ethanol. Prior to spraying, the substrates were pre-heated at 250 ºC.

2.2 Feedstock and Suspensions

To prepare the suspensions, a mix of two commercial powders, alpha-Al_2O_3 AKP30 supplied by Sumitomo Chemical Corp. (Tokyo, Japan) and rutile-TiO_2 K2300 supplied by Kronos (Leverkusen, Germany), was used. According to technical specifications from suppliers, both powders have an average particle size of 300 nm. The powder concentration (solid content) in the ethanol suspension was maintained at 10 %wt. This value was found to allow the best coating cohesion. For suspension stability, an electrosteric dispersant of 2 %wt to powder weight was utilized. This dispersant percentage results in the lowest viscosity, 0.02 mPa·s, and also assures the sedimentation stability for more than 3 days. In each case, the dispersant is burned and disintegrated during the spraying procedure. Other technical details of the preparation and stabilization of suspensions can be found in our previous work [25].

In this study, five alcoholic suspensions of 10 %wt solid content were prepared by adding TiO_2 in the Al_2O_3 suspension, resulting in the following weight percent

compositions: 100 % TiO_2, 13 % TiO_2 + 87 % Al_2O_3, 40 % TiO_2+60 % Al_2O_3, 75 % TiO_2+25 % Al_2O_3 and 100 % Al_2O_3.

2.3 Microscopy Characterization Techniques

The microstructure and fracture surface of the cross-section of coatings were observed by field emission scanning electron microscopy (*FESEM*, JEOL 7400F). Previous to the fracture procedure, samples were submerged in a mix of nitric and sulfuric acid bath in order to dissolve the metallic substrate. For the metallographic preparation, samples were embedded in epoxy resin to provide a support for cutting the cross-section and avoid the detachment of the coating from the substrate. Subsequently, the cross-sections were polished with silicon carbide abrasive papers, following a sequence from 250 to 1000 grit. The final polish was performed with 3 and 1 µm diamond suspensions.

2.4. Mechanical characterization

Coating hardness (H) and elastic modulus (E) were measured using a nanoindenter (G-200, Agilent Technology, USA) with a Berkovich diamond tip. The area function of the indenter was previously calibrated with fused silica as reference material. An array of 25 indentations was performed at a constant 300 nm depth on arbitrary zones of the cross-section, ensuring that a representative zone was analyzed. The location of each test was guided by an optical microscope. Only in cases where coatings were found very fragile (high porosity or low density), the indentation depth was reduced below 150 nm and tests were guided by images of the coating topography using the Nanovision

technology [29]. The images obtained by this method served to choose locations far from pores or defects for nanoindentation tests. The stiffness was obtained by using the Continuous Stiffness Measurement (CSM) method that allows the calculation of the hardness and elastic modulus profiles [30].

3. Results and discussion

3.1. Microstructure characterization

For a coating obtained by APS, it is expected that the typical, well-defined splat microstructure and also vertical, inter-lamellar and intra-lamellar cracks should be observed under secondary electron observation [31]. Furthermore, a bonding coat or a rough substrate surface is required to enhance the cohesion between coating and substrate. Figure 1 shows the cross-sections of coatings obtained by SPS under different TiO_2/Al_2O_3 compositions. A first visual inspection of the images reveals an absence of a well-defined microstructure and of the above-described failures. An outstanding adhesion to the substrate without aid of a bonding layer can be highlighted.

FIGURE 1. Secondary electron images of the sprayed coatings.

With the increment in TiO_2 content, two effects were observed: diminution of coating thickness and increase of coating density. These effects are attributed to a lower melting point and higher specific heat of TiO_2 with respect to Al_2O_3. In fact, due to its lower melting point, TiO_2 acts as a particle binder for Al_2O_3, wrapping its particles during the process. It can be noted that the thickness

decreases from 25 μm to 12 μm when shifting from a composition of 100 %wt Al_2O_3 to 100 %wt TiO_2, resulting in an inversely proportional relationship between Al_2O_3 content and coating density.

Figure 2 shows the electron back scattering (BSE) image of the 60 %wt Al_2O_3-40 %wt TiO_2 coating. The light grey scale contrast obtained from BSE allows the differentiation of areas based on atomic weight; hence, darker regions will represent splats rich in aluminium, while light grey layers correspond to heavier elements such as titanium.

FIGURE 2. Back-scattered electron image of the a) top view and b) polished cross-section view of the 60 %wt Al_2O_3+40 %wt TiO_2 coating.

From the BSE detector, the microstructure was revealed as the typical splat morphology but with very thin and highly diluted grains. This image demonstrates that a high homogeneous distribution of elements exists inside the coating and the cohesion between splats is high enough for coating growth. The most important achievement has been the attainment of a nanometric microstructure within the coating, as Figure 3 reveals.

FIGURE 3. SEM fracture surface image of the 60 %wt Al_2O_3+40 %wt TiO_2 coating at two magnifications.

Figure 3 corresponds to a representative fracture surface of the 60 %wt Al_2O_3+40 %wt TiO_2 coating. At higher magnifications, the submicron and nanometric structure of the particles was revealed, matching the initial size of the grain feedstock. This observation demonstrates that, under the chosen spraying conditions in this work, the SPS technique is a powerful tool to produce nanostructured coatings.

3.2. Mechanical characterization

Modulus and hardness, as properties that play a key role in controlling the response under deformation of any surface [32], need to be paid close attention. The hardness (H) and elastic modulus (E) of coatings were studied by nanoindentation. Indentation tests on coatings with a low content of TiO_2 required the use of a topographic image capturing technology to guide and locate tests due to the poor density of these coatings. Figure 4 shows a representative image of the coating cross-section revealing the performed Berkovich imprints. This technique was very useful to assure that tests were done far from pores and defects.

FIGURE 4. Topographic image acquired on the cross-section of 100 %wt Al_2O_3 coating. The performed Berkovich imprints are marked with arrows.

The H and E in-depth curves obtained for each studied coating are displayed in Figures 5a and 5b, respectively. The error bars were obviated in the elastic modulus graph for a clearer presentation. Several conclusions can be extracted from these curves. At low ranges of tested loads (penetration depth), the

highest value of hardness is found on pure Al_2O_3, as expected for this material [33,34]. Over this range of depths, values of 25 and 350 GPa for H and E, respectively, were obtained. When increasing the load, H an E values drop drastically. It is noticeable that response of the elastic modulus begins to decrease at a lower range of depth and more sharply than the corresponding hardness curve. This behaviour is due to the bigger volume of the elastic stress field beneath the indenter when compared to the residual stresses of the plastic field volume. Thereby, pores around the indent are detected at a lower depth range in elastic response. In this sense, as the addition of TiO_2 increases, the coating density, indentation hardness and elastic modulus are also enhanced. The coating with 40 %wt TiO_2 content revealed constant in-depth values of H and E. This concentration has been then considered as optimal in this work, where values of 17 and 240 GPa for H and E, respectively, have been achieved. The 75 %wt TiO_2 concentration resulted on a hardness of 18 GPa and an elastic modulus of 250 GPa. These values are in accordance with reported nanoindentation studies on Al_2O_3-TiO_2 coatings [33-36]. Figure 6 summarizes the evolution of H and E (over the 150-250 nm range) as a function of TiO_2 content.

FIGURE 6. Hardness and elastic modulus obtained by nanoindentation as a function of TiO_2 %wt content.

An important conclusion that can be drawn from these curves is that H and E values increase in direct proportion to TiO_2 content due to the enhanced

densification effect. This behaviour leads to the conclusion that, as expected, the resultant H and E values obtained by indentation depends strongly on the density of the coating and not so much on the intrinsic properties of the projected material. Nevertheless, our group previously reported [26] that the wear rate of Al_2O_3-TiO_2 coatings is inversely proportional to TiO_2 content. From these results, we conclude that a compromise in composition must be found so the wear resistance and the conditions for obtaining dense coatings with projection techniques are optimized. This investigation should be considered in upcoming studies. In this work, the experimented concentrations serve as an approximate reference for the resulting density and mechanical properties that should be finally obtained by SPS when employing low-concentration Al_2O_3-TiO_2 alcoholic suspensions as feedstock.

Conclusions

The deposition of nano-sized Al_2O_3 by SPS technique using a low concentrated alcoholic suspension generates low-density coatings that are unable to support minimal mechanical efforts. Addition of TiO_2 in the suspension permits to obtain denser coatings while maintaining nanostructural features. We have demonstrated that TiO_2 acts as a flux agent in the presence of Al_2O_3. By tuning the ratio of Al_2O_3/TiO_2 content, it is possible to predict and control the density of the coating and, hence, the mechanical properties. Under the selected process conditions, a homogeneously distributed and very thin lamellar Al_2O_3/TiO_2 microstructure composed by nanostructured material was obtained.

References

[1] B.H. Kear, Z. Kalman, R.K. Sadangi, G. Skandan, J. Colaizzi, W.E. Mayo, J. Therm. Spray Technol. 9 (4) (2000) 483.

[2] S.C. Tjong and H. Chen, Materials Science and Engineering R: Reports 45 (1-2) (2004) 1.

[3] A. Bellosi, D. Sciti, S. Guicciardi, Journal of the European Ceramic Society 24 (12) (2004) 3295.

[4] L. Pawlowski, Surface and Coatings Technology 202 (18) (2008) 4318.

[5] T. Cosack, L. Pawlowski, S. Schneiderbanger, S. Sturlese, Journal of Engineering for Gas Turbines and Power 116 (1) (1994) 272.

[6] L. Pawlowski, Powder Metallurgy International 23 (6) (1991) 357.

[7] Y. Liu, F.-. Min, J.-. Zhu, M.-. Zhang, Materials Science and Engineering A 546 (2012) 328.

[8] R. Benavente, M.D. Salvador, F.L. Penaranda-Foix, E. Pallone, A. Borrell, Ceram. Int. 40 (7 PART B) (2014) 11291.

[9] B.-. Li, D.-. Liu, J.-. Liu, S.-. Hou, Z.-. Yang, Ceram. Int. 38 (5) (2012) 3693.

[10] A. Borrell, M.D. Salvador, V.G. Rocha, A. Fernández, T. Molina, R. Moreno, Composites Part B: Engineering 47 (2013) 255.

[11] F.-. Trifa, G. Montavon, C. Coddet, Surface and Coatings Technology 195 (1) (2005) 54.

[12] C. Kim, Y.S. Heo, T.W. Kim, K.S. Lee, Journal of the Korean Ceramic Society 50 (5) (2013) 326.

[13] L. Latka, S.B. Goryachev, S. Kozerski, L. Pawlowski, Materials 3 (7) (2010) 3845.

[14] H. Kassner, R. Siegert, D. Hathiramani, R. Vassen, D. Stoever, J. Therm. Spray Technol. 17 (1) (2008) 115.

[15] P. Fauchais, V. Rat, J.-. Coudert, R. Etchart-Salas, G. Montavon, Surface and Coatings Technology 202 (18) (2008) 4309.

[16] L. Pawlowski, Surface and Coatings Technology 203 (19) (2009) 2807.

[17] A. Joulia, G. Bolelli, E. Gualtieri, L. Lusvarghi, S. Valeri, M. Vardelle, S. Rossignol, A. Vardelle, Journal of the European Ceramic Society 34 (15) (2014) 3925.

[18] P. Carpio, E. Rayón, L. Pawlowski, A. Cattini, R. Benavente, E. Bannier, M.D. Salvador, E. Sánchez, Surface and Coatings Technology 220 (2013) 237.

[19] E. Bannier, G. Darut, E. Sánchez, A. Denoirjean, M.C. Bordes, M.D. Salvador, E. Rayón, H. Ageorges, Surface and Coatings Technology 206 (2-3) (2011) 378.

[20] S. Kozerski, F.-. Toma, L. Pawlowski, B. Leupolt, L. Latka, L.-. Berger, Surface and Coatings Technology 205 (4) (2010) 980.

[21] M. Gardon and J.M. Guilemany, J. Therm. Spray Technol. 23 (4) (2014) 577.

[22] H.-. Wang, J.-. Ma, G.-. Li, J.-. Kang, B.-. Xu, Appl. Surf. Sci. 314 (2014) 468.

[23] D. Chen, E.H. Jordan, M. Gell, Appl. Surf. Sci. 255 (11) (2009) 5935.

[24] R.S. Lima and B.R. Marple, J. Therm. Spray Technol. 16 (1) (2007) 40.

[25] G. Darut, E. Klyatskina, S. Valette, P. Carles, A. Denoirjean, G. Montavon, H. Ageorges, F. Segovia, M. Salvador, Mater Lett 67 (1) (2012) 241.

[26] E. Klyatskina, L. Espinosa-Fernández, G. Darut, F. Segovia, M.D. Salvador, G. Montavon, H. Agorges, Tribology Letters 59 (1) (2015)

[27] V.P. Singh, A. Sil, R. Jayaganthan, Materials and Design 32 (2) (2011) 584.

[28] N. Dejang, A. Watcharapasorn, S. Wirojupatump, P. Niranatlumpong, S. Jiansirisomboon, Surface and Coatings Technology 204 (9-10) (2010) 1651.

[29] V. Bonache, E. Rayón, M.D. Salvador, D. Busquets, Materials Science and Engineering A 527 (12) (2010) 2935.

[30] W.C. Oliver and G.M. Pharr, J. Mater. Res. 7 (6) (1992) 1564.

[31] H. Podlesak, L. Pawlowski, J. Laureyns, R. Jaworski, T. Lampke, Surface and Coatings Technology 202 (15) (2008) 3723.

[32] A.M. Korsunsky and A. Constantinescu, Materials Science and Engineering A 423 (1-2) (2006) 28.

[33] S. Ruppi, A. Larsson, A. Flink, Thin Solid Films 516 (18) (2008) 5959.

[34] E. Rayón, V. Bonache, M.D. Salvador, E. Bannier, E. Sánchez, A. Denoirjean, H. Ageorges, Surface and Coatings Technology 206 (10) (2012) 2655.

[35] E. Bannier, M. Vicent, E. Rayón, R. Benavente, M.D. Salvador, E. Sánchez, Appl. Surf. Sci. 316 (1) (2014) 141.

[36] I.G. Cano, S. Dosta, R. Caldeira, J.R. Miguel, J.M. Guilemany, Materials Science Forum 587-588 (2008) 153.

FIGURE CAPTIONS

Figure 1. Secondary electron images of the sprayed coatings.

Figure 2. Back-scattered electron image of the a) top view and b) polished cross-section view of the 60 %wt Al_2O_3+40 %wt TiO_2 coating.

Figure 3. SEM fracture surface image of the 60 %wt Al_2O_3+40 %wt TiO_2 coating at two magnifications.

Figure 4. Topographic image acquired on the cross-section of 100 %wt Al_2O_3 coating. The performed Berkovich imprints are marked with arrows.

Figure 5. Hardness in-depth curves (a) and elastic modulus curves (b) acquired by nanoindentation on the polished cross-section coatings. The error bar was omitted in b) for a clearer presentation.

Figure 6. Hardness and elastic modulus obtained by nanoindentation as a function of TiO_2 %wt content.

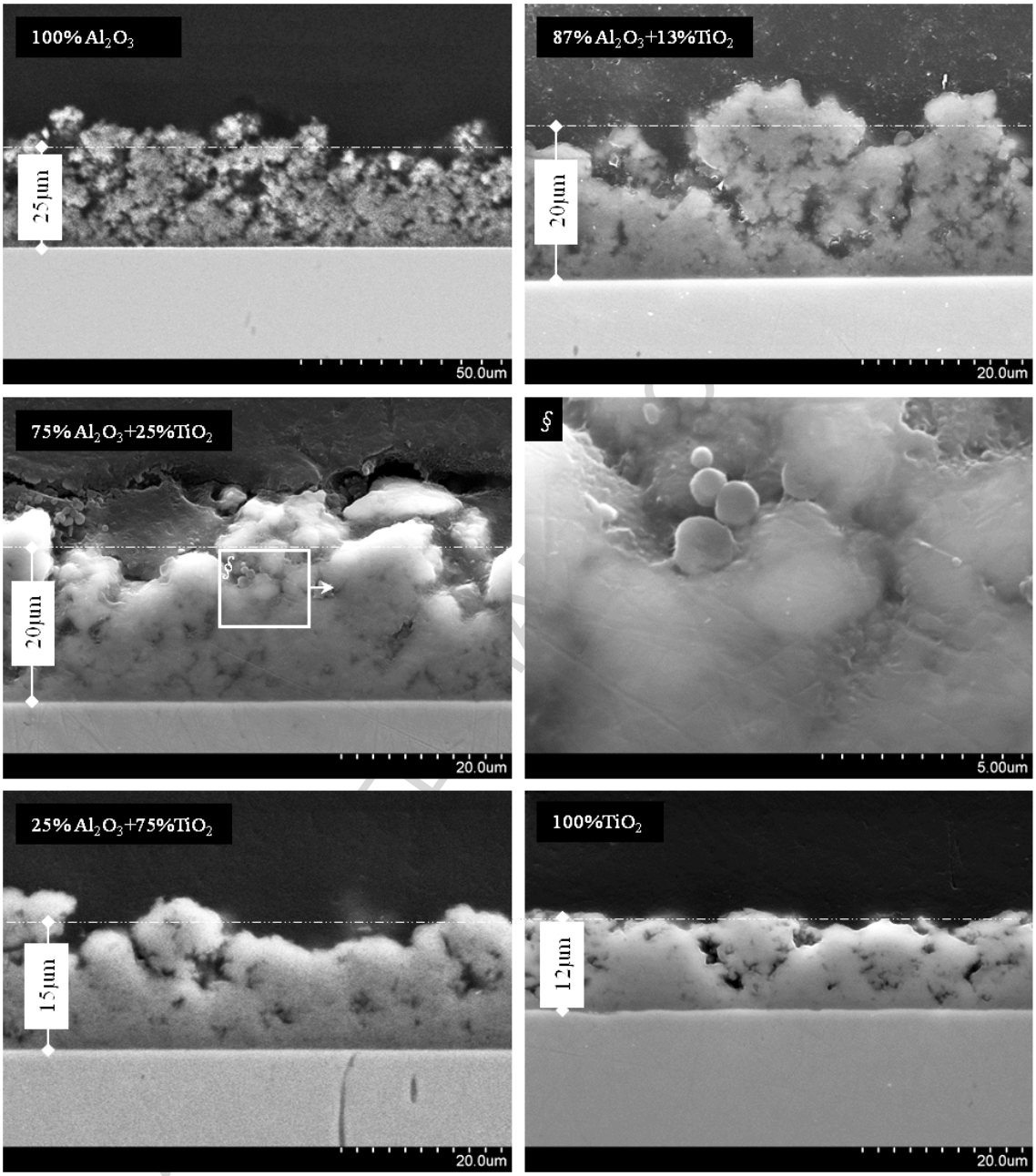

Fig. 1

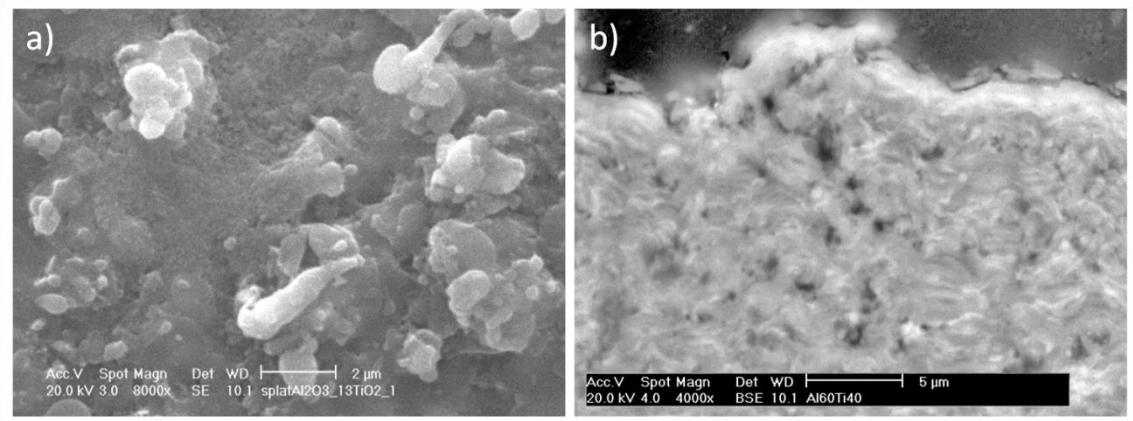

Fig. 2

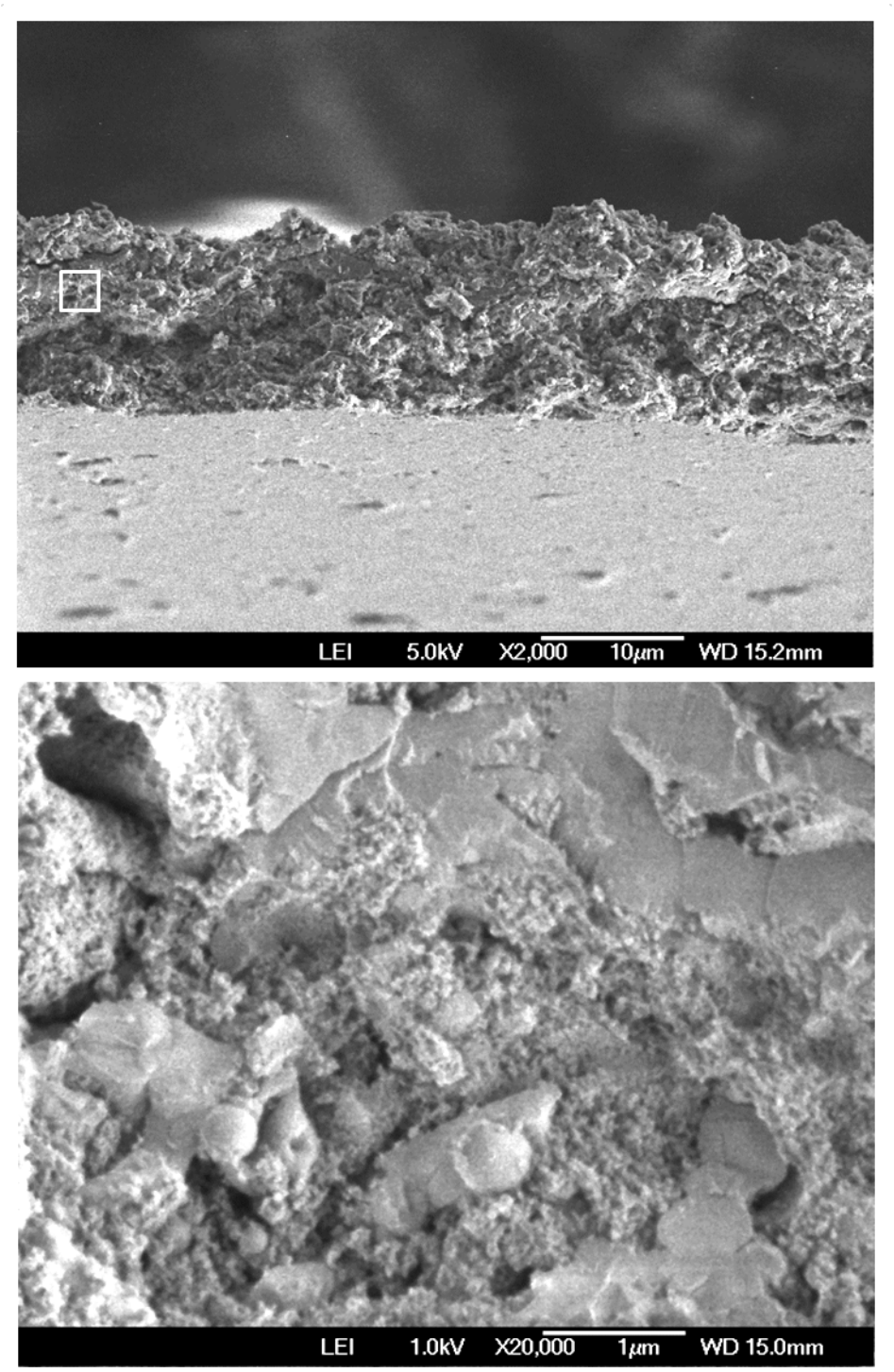

Fig. 3

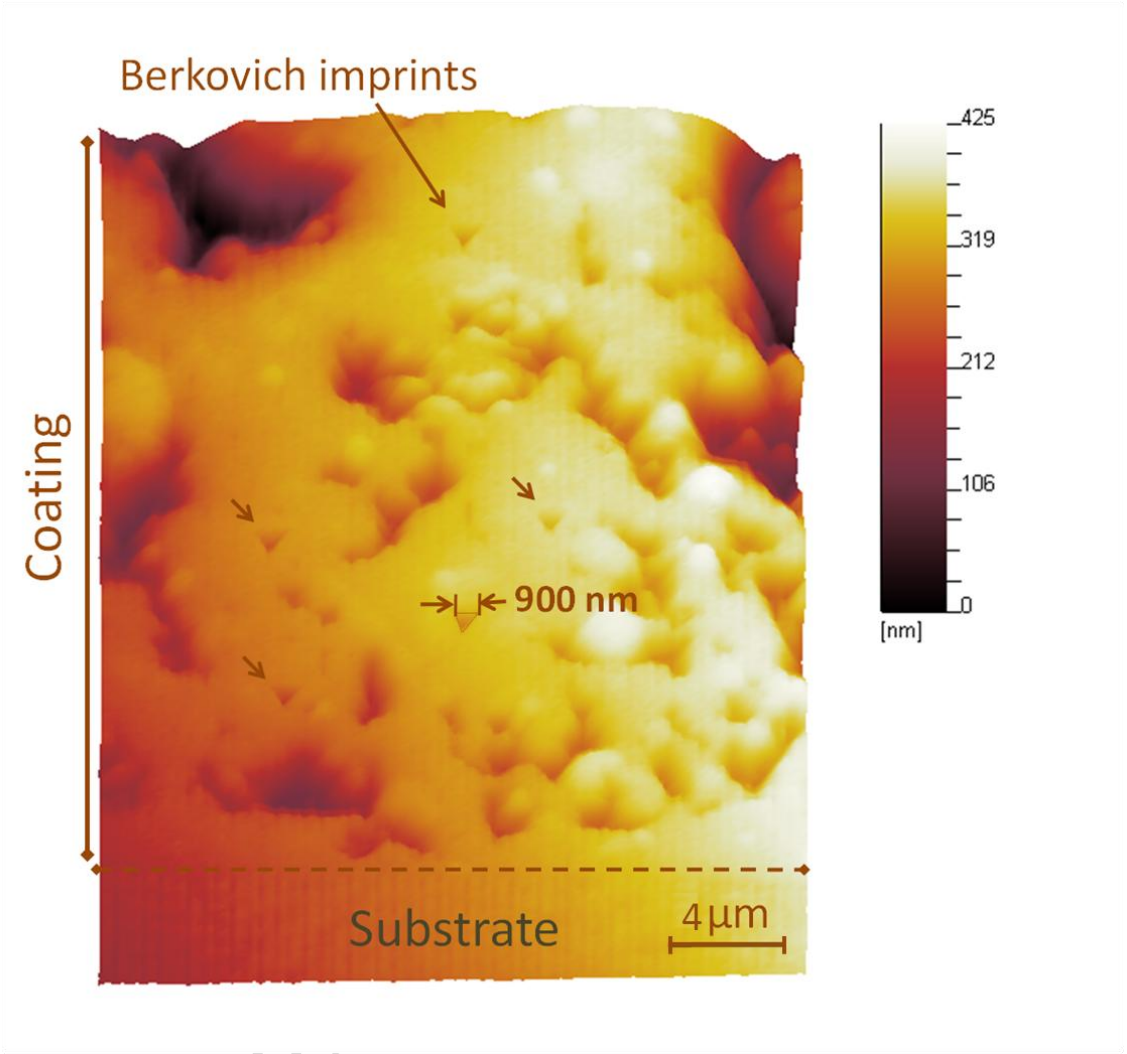

Fig. 4

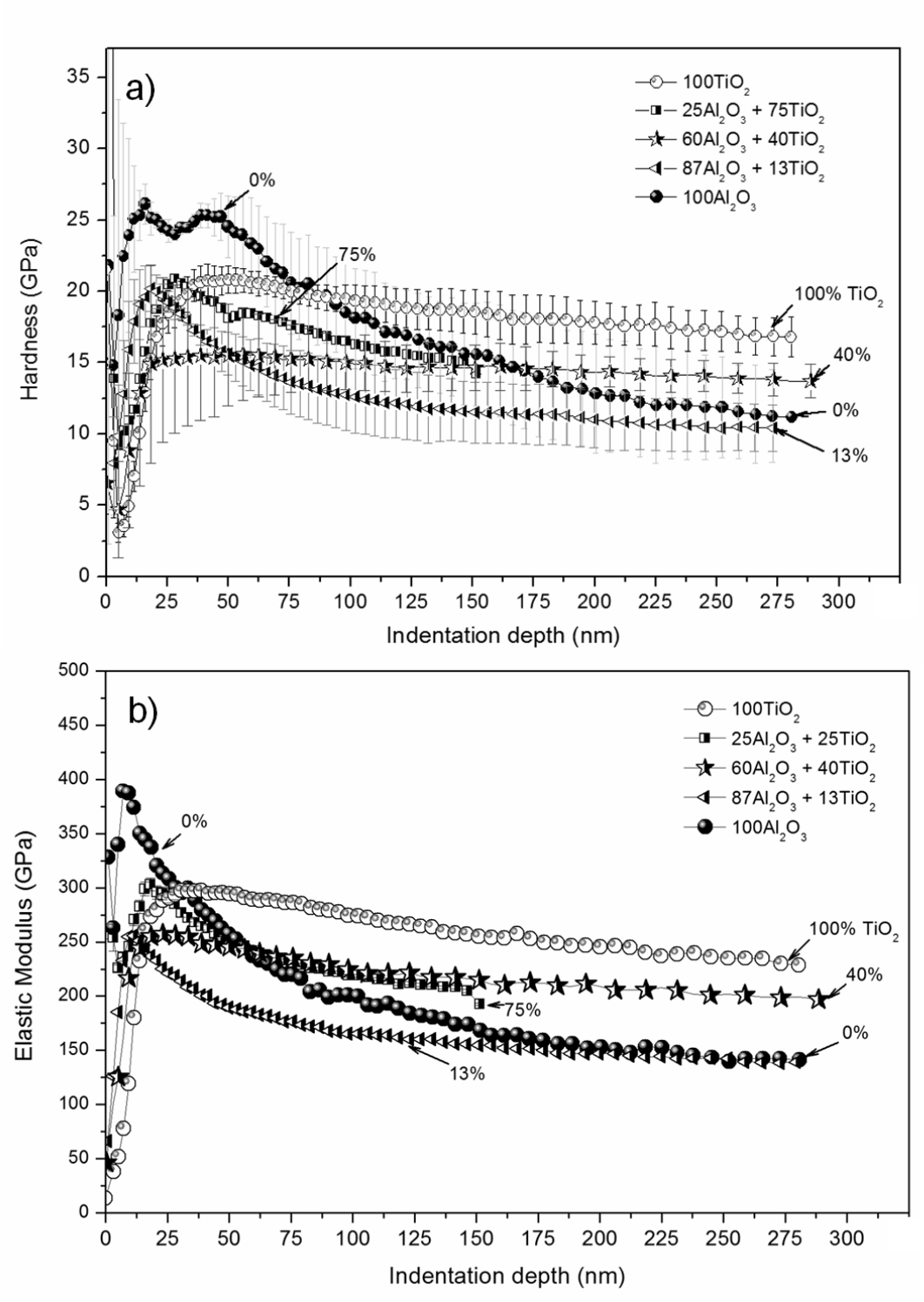

Fig. 5

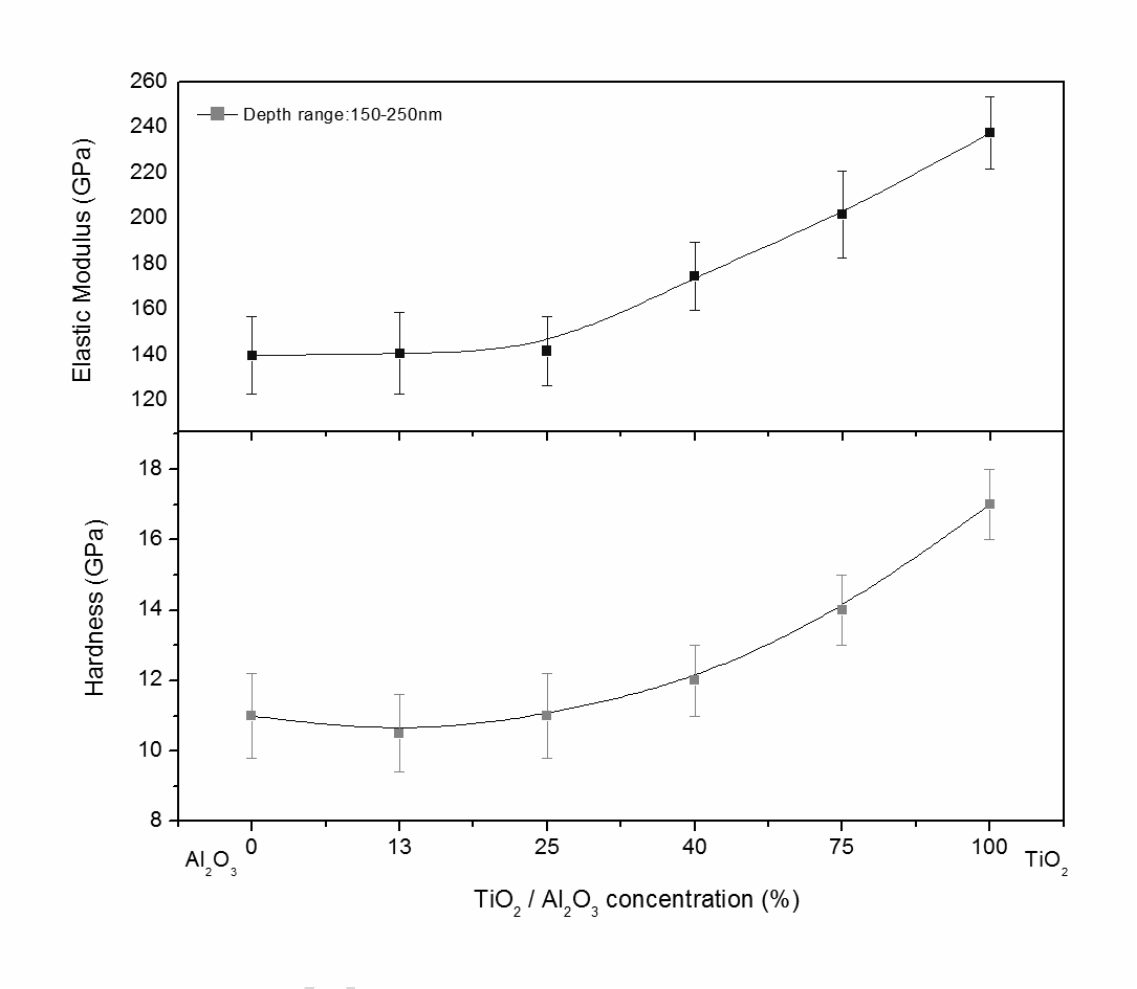

Fig. 6

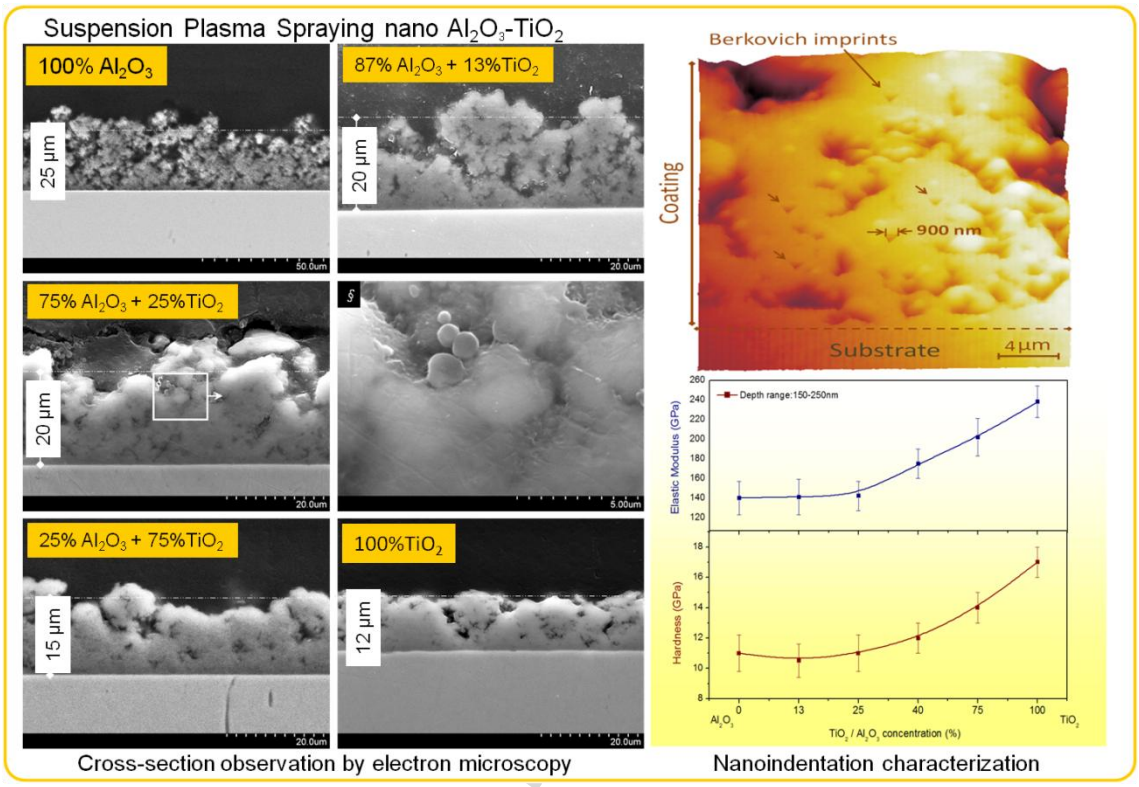

Graphical abstract

Highlights

- Al_2O_3-TiO_2 coatings with retained nanostructure were obtained by SPS
- TiO_2 acts as a flux agent in the presence of Al_2O_3
- Density and hardness of coatings increase with TiO_2 content